JACS Au
AN OPEN ACCESS JOURNAL OF THE AMERICAN CHEMICAL SOCIETY

pubs.acs.org/jacsau

Article

Liquid Crystalline Magneto-Optically Active Peralkylated Azacoronene

Léo Delage-Laurin and Timothy M. Swager*

Cite This: *JACS Au* 2023, 3, 1965−1974

Read Online

ACCESS | Metrics & More | Article Recommendations | Supporting Information

ABSTRACT: Organic Faraday rotators have gained significant attention in recent years as a promising alternative to traditional inorganic magneto-optical (MO) materials as a result of their lower cost, superior mechanical properties, and potential for large-scale deployment. This interest is peaked by the fact that a number of high symmetry, rigid, strongly optically absorbing organic chromophores display Verdet constants an order of magnitude higher than commercial inorganic Faraday rotators. Critical to the development of new generations of organic materials is the ability to organize them in optimal structures for optical coupling/measurements. We report herein the synthesis of a dodecyl-substituted hexapyrrolohexaazacoronene (**C_{12}-HPHAC**) displaying discotic liquid crystalline (LC) properties and large Faraday rotation. Thin films with a redox mixed **C_{12}-HPHAC/C_{12}-HPHAC^{+2}** composition display a discotic columnar LC phase, are stable to air and moisture in the solid and solution states, and achieve a maximum Verdet constant of 3.36×10^5 deg T^{-1} m^{-1} at 700 nm. This result is consistent with Serber's model of magnetic circular birefringence and displays one of the largest reported Verdet constants for organic materials in the UV−Vis range. The LC phase aligns the molecules and leads to gains in Verdet constants of up to 105% through the favorable orientation of the molecules' magnetic and electric transition dipole moments with respect to the applied magnetic field.

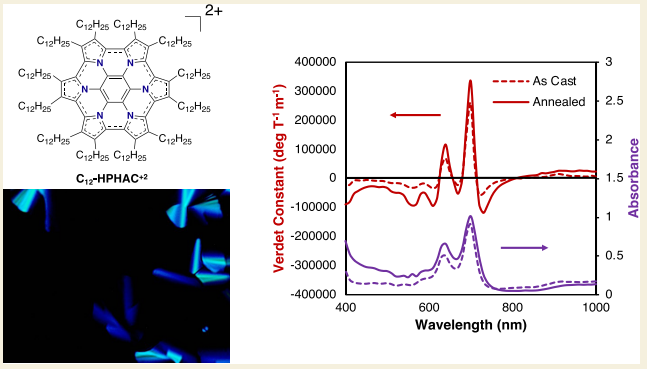

KEYWORDS: *Faraday rotation, azacoronene, polycyclic aromatic hydrocarbons, liquid crystals, Verdet constant*

INTRODUCTION

Pyrrole-fused compounds are molecular scaffolds containing several pyrrole rings that are fused together or annulated with other aromatic or heterocyclic ring systems. These heterocyclic nanographene motifs[1,2] offer unique electronic, photophysical, redox, and biological properties and therefore are potential candidates for applications ranging from organic electronics,[3−6] sensing,[7−9] and even as substructures of potential drug candidates.[10−12] Additionally, they often exhibit high thermal stability and are chemically robust.[6,7,13−15] Azacoronenes, a subclass of pyrrole-fused compounds, are of particular interest for their optical and redox properties.[2,13] These molecules are characterized by a structure that consists of a central benzene core substituted by six fused pyrrole rings. The synthesis of unsubstituted hexapyrrolohexaazacoronene (**HPHAC**) (Figure 1) was initially attempted by Lazerges et al.[16] via the oxidation of hexapyrrolylbenzene with iron(III) perchlorate; however, only partially oxidized species were observed by matrix-assisted laser desorption/ionization time-of-flight (MALDI-TOF) mass spectrometry. A subsequent study by Takase et al.[13] demonstrated that alkyl substitution at the periphery increased solubility, prevented intermolecular couplings, and allowed for the isolation and characterization of both the neutral and dication species. Chemical modification of the peripheral substituents, the inner core, and via π-extension have since led to many other analogs.[7,14,15,17−22] These studies highlighted the aromaticity of **HPHAC** derivatives and their ability to display multiple stable oxidation states.

The Faraday effect, which results in the rotation of the plane of polarization of linearly polarized light after passing through a magnetized medium,[23] has not yet been reported for **HPHACs**. This phenomenon occurs through the interaction of the magnetic field with the medium, causing the light wave's electric field vector to rotate. The extent of the rotation is characterized by a material's Verdet constant (deg T^{-1} m^{-1}), which is proportional to the magnetic field strength and the optical path length through the medium. For a discussion of molecular systems, we refer the reader to the published

Received: May 1, 2023
Revised: June 27, 2023
Accepted: June 27, 2023
Published: July 8, 2023

https://doi.org/10.1021/jacsau.3c00212
JACS Au 2023, 3, 1965−1974

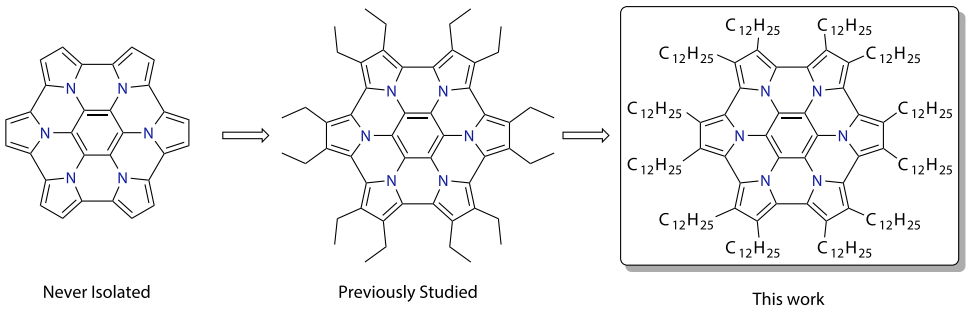

Figure 1. Hexapyrrolohexaazacoronene (HPHAC) and peralkylated analogs.

perspective on Faraday rotation by Nelson et al.[23] Faraday rotators have found utility as a probing tool in the fields of radio astronomy[24−26] and plasma physics.[27−29] Additional applications include remote magnetic-field sensing,[30−32] MO imaging,[33−35] optical communication technology,[36,37] and optical isolation.[38−40] Currently, inorganic materials rich in paramagnetic heavy elements dominate commercial applications and fundamental research.[41,42] However, organic materials are potential materials that could further diversify applications with demonstrated Verdet constants roughly one order of magnitude larger than their inorganic counterparts.[43−46] One approach to achieve high Verdet constants in organic materials is to create high symmetry, rigid π-electronic systems exhibiting narrow absorption bands with large extinction coefficients. In these types of materials, the large Verdet constants are understood to mainly originate from an A-term Faraday rotation mechanism.[23] Nitrogen-rich PAHs such as **HPHACs** fulfill these molecular requirements when oxidized and possess multiple stable oxidation states displaying strong absorption bands,[15] making them ideal candidates as Faraday rotators. The rich and robust redox properties of alkyl-substituted **HPHACs** could also allow for tunable, wavelength-dependent Faraday rotation based on the oxidation state. The mechanism by which such molecules display large magneto-optical rotation is in essence a resonance-enhanced process, which means it will likely be associated with large UV−Vis absorption as well. Nonetheless, we believe that these molecules may find utility in certain applications such as magneto-optical imaging and magnetic-field sensing where optical output is not paramount.

The synthesis of **HPHAC** derivatives that can yield high-quality optical films is essential. The study of the optical properties of **HPHACs** in the solid state has not been reported to date, but previous reports mentioned their low solubility as a limitation for the fabrication of thin films.[15,47] Furthermore, the crystallinity of previously reported **HPHAC** derivatives, which is enhanced in the ionic oxidized states, further complicates formation of optical quality (non-scattering) films.[46] To address this issue, we synthesize a peralkylated **HPHAC** substituted with dodecyl alkyl chains ($\mathbf{C_{12}}$**-HPHAC**), which achieves two purposes. First, it increases solubility of the compound in organic solvents and allows for the fabrication of thin films by spin-coating and drop-casting. Second, the installation of long alkyl chains lowers the melting point of the materials and imparts liquid crystallinity. Other alkyl chain lengths would likely be adequate and lead to liquid crystalline properties; however, we chose dodecyl as a starting point as we intuitively hypothesized that it would lead to both great solubility and liquid crystalline properties at room temperature. Liquid crystalline organizations have been reported to increase Faraday rotation via the molecular alignment of thin film samples.[44,45,48] We find that the neutral $\mathbf{C_{12}}$**-HPHAC** and dication $\mathbf{C_{12}}$**-HPHAC**$^{+2}$ do not display a liquid crystalline (LC) phase; however, thin films with a mixed $\mathbf{C_{12}}$**-HPHAC**/$\mathbf{C_{12}}$**-HPHAC**$^{+2}$ composition display a columnar LC phase. When thermally annealed above the isotropic transition and slowly cooled down to 20 °C, samples of $\mathbf{C_{12}}$**-HPHAC**/$\mathbf{C_{12}}$**-HPHAC**$^{+2}$ show a significant increase in Faraday rotation over spin-coated thin films. Specifically, slow cooling of the isotropic phase (1°/min) results in a 30% increase in Verdet constant at 700 nm, reaching 3.36×10^{-5} deg T^{-1} m^{-1}. This organization produces an even larger increase in the Verdet constant at 730 nm (105%), corresponding to the shoulder of the A-term Faraday response and at the edge of the optical band reaching -1.1×10^{-5} deg T^{-1} m^{-1}. We attribute the increases in Verdet constant to a homeotropic alignment of the columns with respect to the glass substrate. The semi-quantitative expressions of the Faraday A-term in Serber's model of magnetic circular birefringence (MCB)[23] refer to a coordinate system, suggesting that the orientation of the magnetic dipole moments and the electric transition dipole moments can impact Faraday rotation in solid-state samples. Therefore, optimally ordered chromophores show enhanced Verdet constants relative to materials with randomly ordered molecular axes. The orientation and LC properties of the samples were confirmed via polarized-light optical microscopy (POM). The Verdet constant of 3.36×10^{-5} deg T^{-1} m^{-1} displayed by the annealed $\mathbf{C_{12}}$**-HPHAC**/$\mathbf{C_{12}}$**-HPHAC**$^{+2}$ thin film is among the largest reported to date for an organic material.

RESULTS AND DISCUSSION

The synthesis of alkyl-substituted **HPHACs** involves a 6-fold nucleophilic aromatic substitution addition of the pyrrole anions to hexafluorobenzene followed by a 6-fold oxidative cyclodehydrogenation reaction (Scholl reaction).[13,15] This synthetic route has been used for a number of fused polycyclic aromatic hydrocarbons containing heterocycles and is used here for the synthesis of $\mathbf{C_{12}}$**-HPHAC**. We first synthesized the permethylated analog of **HPHAC** before embarking on the synthesis of the more challenging $\mathbf{C_{12}}$**-HPHAC** to validate our hypothesis regarding the Faraday rotation potency of the structure. In a recent report, Oki et al.[15] measured the magnetic circular dichroism of ethyl-substituted **HPHAC**, indicating that such a molecule could exhibit large Faraday rotation. The synthesis of pyrrole monomers substituted exclusively at the β-positions requires multiple steps as electrophilic substitution of the pyrrole ring occurs preferentially at the more reactive α-positions.[49] Selective β-substitution on pyrrole is not feasible as it will also lead to

https://doi.org/10.1021/jacsau.3c00212
JACS Au 2023, 3, 1965−1974

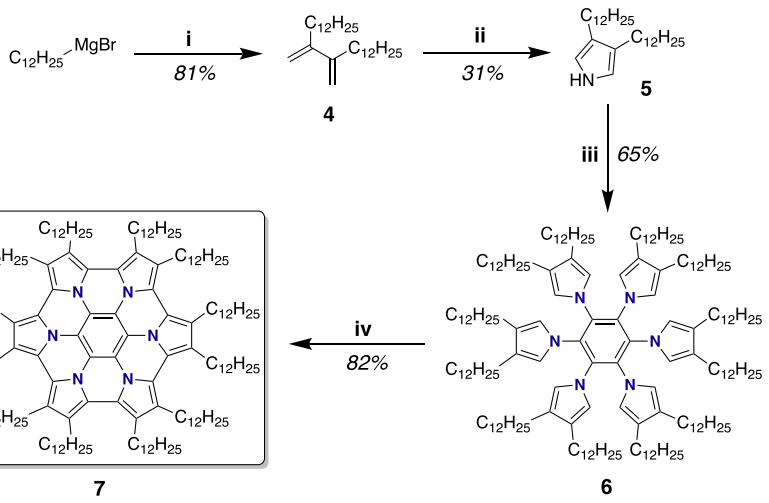

Figure 2. Synthetic route to **C_{12}-HPHAC**. Reactions and conditions are as follows: (i) CuI, THF at 0 °C for 30 min, then 1,4-dichloro-2-butyne at rt for 2 h; (ii) methyl carbamate, $SOCl_2$, pyridine, and PhMe at reflux for 3 h, then KOH and MeOH at reflux for 2 h; (iii) NaH and dimethylformamide at 0 °C for 1 h, then C_6F_6 at rt for 12 h; (iv) DDQ, TfOH, and dichloromethane at 0 °C for 3 h.

some extent of substitution in the α-positions and mixtures of regioisomers are hard to separate. The use of sterically bulky protecting groups on the pyrrole nitrogen can impede reactions at the α-position but leads to mixtures of 3- and 3,4-substituted products, which also results in difficult separations and provides low overall yields of the di-substituted products.[50]

3,4-Dimethyl-1*H*-pyrrole **1** was efficiently synthesized following a previously reported literature procedure by Ichimura et al.[51,52] wherein 2,3-dimethylbutadiene undergoes a Diels−Alder reaction with sulfinylcarbamic acid methyl ester. The latter is readily prepared in situ through the reaction of methyl carbamate with thionyl chloride and pyridine. The cycloaddition yielded 2-methoxycarbonyl-3,6-dihydro-4,5-dimethyl-1,2-thiazine 1-oxide (see Figure S1), which was used without purification as a result of its moisture sensitivity. The target 3,4-dimethyl-1*H*-pyrrole **1** was obtained in 30% yield via a reaction cascade induced with potassium hydroxide in methanol at reflux to give reduction in ring size (6- to 5-member ring) to the aromatized pyrrole (Figure S1). The six-fold SNAr addition reaction of the anion of 3,4-dimethyl-1*H*-pyrrole **1**, generated by reaction with sodium hydride in dimethylformamide, with hexafluorobenzene, produces 1,2,3,4,5,6-hexakis(3,4-dimethyl-1*H*-pyrrol-1-yl)benzene **2** in 81% yield. In a final step, 1,2,3,4,5,6-hexakis(3,4-dimethyl-1*H*-pyrrol-1-yl)benzene **2** was subjected to a 6-fold oxidative cyclodehydrogenation using a combination of 2,3-dichloro-5,6-dicyano-1,4-benzoquinone and triflic acid in DCM at 0 °C for 3 h to produce permethylated **HPHAC 3** in a 79% yield. The mechanism by which the reaction proceeds through likely involves the formation of cationic intermediates.[53,54] Although the purity of permethylated **HPHAC 3** could not be confirmed by NMR due to the insolubility of the compound in all solvents tested, spectroscopic measurements of the absorption and Faraday rotation of the oxidized species were possible due to the increased solubility of the cation radical and dication in many organic solvents. The solution-phase Faraday rotation of the permethylated **HPHAC** was confirmed, yielding an A-term Faraday rotation for the largest absorption band of both the cation and dication (Figure S16). This result was sufficient to move forward with the synthesis of HPHAC analogs with longer alkyl chains.

Longer alkyl chain 3,4-dialkyl-substituted pyrrole monomers are synthesized using a four-step process in approximately 15% yield.[55,56] Most synthetic methods to install shorter alkyl chains at the β-positions are not suited for the installation of longer alkyl chains.[51,57−59] One viable method involves 2,3-alkyl-substituted butadiene intermediates[60] that can be used as a dienophile in the same procedure as employed for **1** to yield the desired pyrrole. This preferred method reduces the number of synthetic steps by half with regard to the previously reported synthesis of 3,4-didodecyl-1*H*-pyrrole **5**[56] with higher yields (Figure 2).

Butadiene 13,14-dimethylenehexacosane **4** was synthesized via a two-fold S_N2' reaction of 1,4-dichloro-2-butyne with dodecylmagnesium bromide. It is reported in the literature that such a reaction does not proceed efficiently using primary alkyl magnesium bromides,[60] but we found that the use of catalytic copper iodide provides the desired product in 81% yield. The formation of pyrrole via Diels−Alder in this two-step method gave 3,4-didodecyl-1*H*-pyrrole **5** in 25% overall yield, which is higher than those reported for other 3,4-dialkyl substituted pyrroles with alkyl chains longer than hexyl. 3,4-Didodecyl-1*H*-pyrrole **5** was deprotonated in dimethylformamide using sodium hydride and then reacted with hexafluorobenzene overnight at room temperature to produce 1,2,3,4,5,6-hexakis-(3,4-didodecyl-1*H*-pyrrol-1-yl)benzene **6** in 65% yield. In the last step, 1,2,3,4,5,6-hexakis(3,4-didodecyl-1*H*-pyrrol-1-yl)-benzene **6** was subjected to the same oxidative cyclization conditions as used for compound **2** to provide **C_{12}-HPHAC 7** in 82% yield. Additional details on the synthetic methods are in the Supporting Information.

The oxidation of neutral **C_{12}-HPHAC** was investigated using a variety of oxidizing agents including nitrosonium tetrafluoroborate ($NOBF_4$), nitrosonium hexafluorophosphate ($NOPF_6$), iron(III) chloride, bromine, and antimony pentachloride ($SbCl_5$). All oxidants yielded some extent of cation and dication species; however, $SbCl_5$ delivered an efficient stoichiometric oxidation. A common solvent that could solubilize both the nitrosonium salts and **C_{12}-HPHAC** was not found, making it difficult to deliver precise molecular equivalents of oxidant. $FeCl_3$ and bromine yielded partial oxidation, and excess of oxidizing agents complicated purification and the formation of well-behaved LC phases.

https://doi.org/10.1021/jacsau.3c00212
JACS Au 2023, 3, 1965−1974

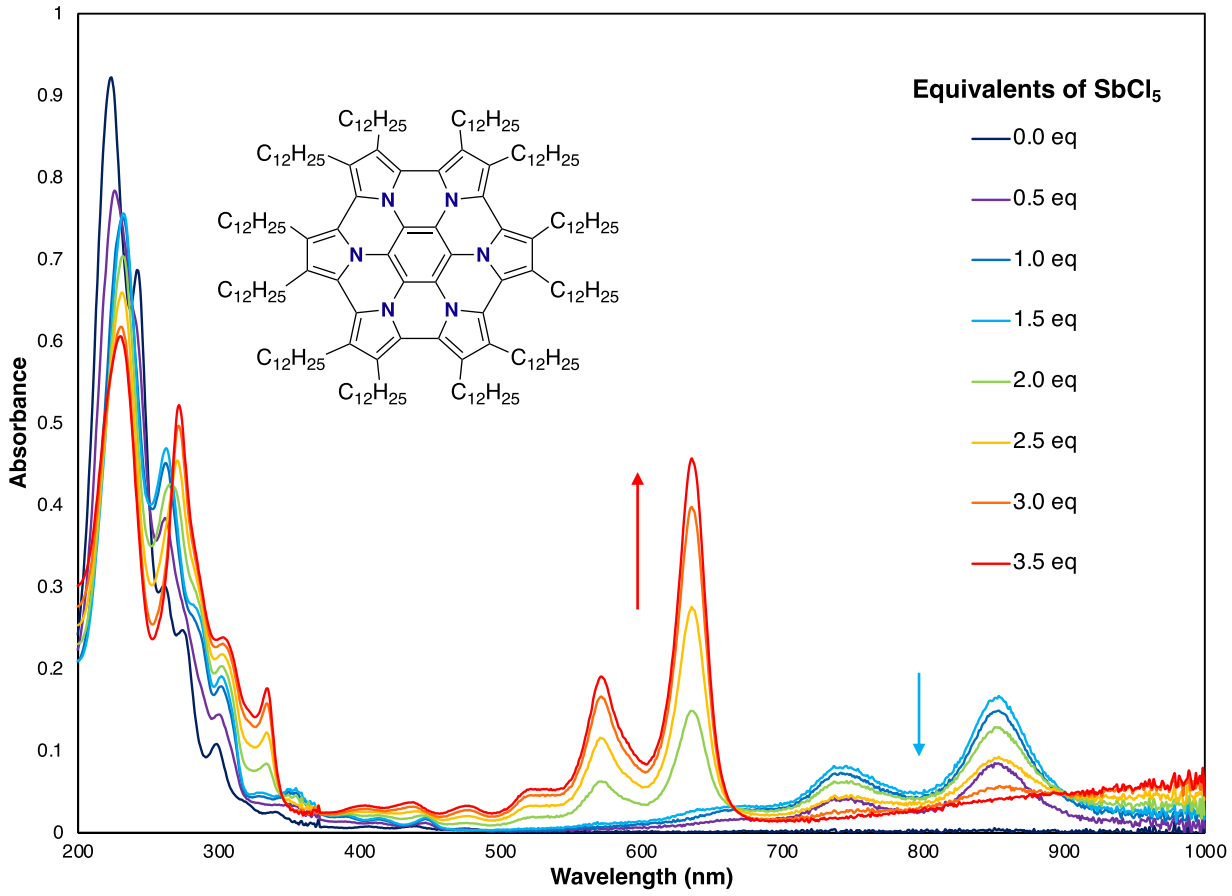

Figure 3. UV−Vis spectra of the redox titration of C_{12}-**HPHAC** with $SbCl_5$.

Redox titration was performed (Figure 3) to determine the number of $SbCl_5$ equivalents needed to achieve precise oxidation of C_{12}-**HPHAC**. We found that 1.5 and 3.0 equiv of $SbCl_5$ lead almost exclusively to the cation radical C_{12}-**HPHAC**$^{+\bullet}$ and the dication C_{12}-**HPHAC**$^{+2}$, respectively. This is consistent with the disproportionation oxidation mechanism of $SbCl_5$, where two $SbCl_6^-$ anions and one molecule of $SbCl_3$ are formed, leading to a 3:2 stoichiometry of $SbCl_5$ to C_{12}-**HPHAC** for complete oxidation.[61] Upon addition of 2.0 equiv of $SbCl_5$, the UV−Vis signature of C_{12}-**HPHAC**$^{+2}$ started to appear. Further addition of $SbCl_5$ above 3.5 equiv did not yield a significant increase in the dication signature or new absorption peaks associated with the trication. Note that without the addition of oxidizing agent, a small amount of C_{12}-**HPHAC**$^{+\bullet}$ is present in the sample, which was observed by UV−Vis and Faraday rotation measurements. Oxidation by atmospheric oxygen is likely the cause of this based on the first oxidation potential of alkyl-substituted **HPHACs** being very close to 0 V. Indeed, cyclic voltammetry of the previously reported ethyl-substituted analog showed the first oxidation event at −0.51 V (CH_2Cl_2, $TBAPF_6$ vs Fc/Fc^+).[15] The addition of anhydrous hydrazine to the solution reduced any cation radical present and yielded neutral clean C_{12}-**HPHAC**.

The Faraday rotation of the neutral and oxidized C_{12}-**HPHAC** species was first explored in solution (Figure 4). The Faraday rotation of a solution of neutral C_{12}-**HPHAC** could not be detected because the strong optical transitions reside at wavelengths below 400 nm, which is less than the wavelength limits of our instrument. When 1.5 equiv of $SbCl_5$ was added, two new major longer wavelength absorption bands appeared, and consistent with previous reports, they are assigned to C_{12}-**HPHAC**$^{+\bullet}$. The largest absorption band at 910 nm yielded a maximum mass specific magnetic rotation in solutions of dichloromethane of 1.4×10^2 deg L g^{-1} T^{-1} m^{-1} with a line shape consistent with a Faraday A-term response. The weaker absorption band at 790 nm yielded lower maximum mass specific magnetic rotations with peak values of 2.7×10^1 deg L g^{-1} T^{-1} m^{-1} at 800 nm and -3.0×10^1 deg L g^{-1} T^{-1} m^{-1} at 770 nm. However, the rotations associated with the 790 nm band display a line shape that is most consistent with a Faraday C-term response.[23]

When 3.0 equiv or more of $SbCl_5$ was added, the optical transitions observed for the cation radical C_{12}-**HPHAC**$^{+\bullet}$ completely disappeared and two new higher intensity blue-shifted absorption bands appeared. The largest absorption band at 690 nm yielded a maximum mass specific magnetic rotation of 1.6×10^2 deg L g^{-1} T^{-1} m^{-1}, with a line shape consistent with a Faraday A-term response. The longer wavelength shoulder of the Faraday A-term response at 710 nm reaches -1.1×10^2 deg L g^{-1} m^{-1} T^{-1}, which is much larger in magnitude than the same type of feature for the cation radical. The weaker absorption band at 630 nm yielded smaller maximum mass specific magnetic rotation of 5.6×10^1 deg L g^{-1} T^{-1} m^{-1} at 640 nm. The line shape of the weaker higher

https://doi.org/10.1021/jacsau.3c00212
JACS Au 2023, 3, 1965−1974

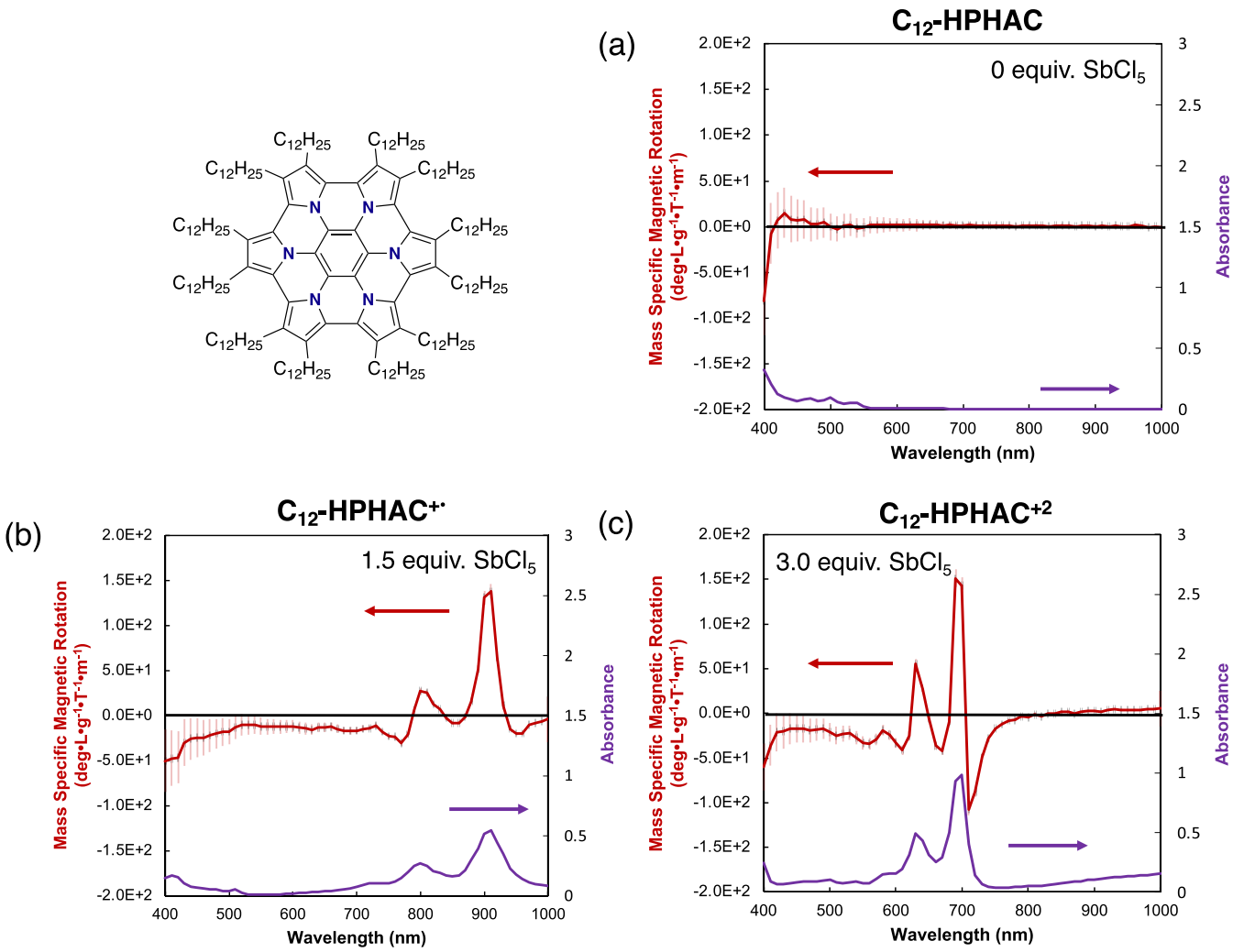

Figure 4. Absorption spectra (purple) and associated Faraday rotation responses (red) of solution-state samples of **C_{12}-HPHAC** with (a) 0 equiv, (b) 1.5 equiv, and (c) 3.0 equiv of $SbCl_5$. All solutions are 2×10^{-4} M in dichloromethane.

energy absorption is consistent with a Faraday A-term response. There are noteworthy similarities between the dispersions and line shapes of the Faraday rotation spectra of **C_{12}-HPHAC$^{+\bullet}$** and **C_{12}-HPHAC^{+2}**. The primary differences are in the absorption band widths and the extinction coefficients, where **C_{12}-HPHAC^{+2}** displays narrower transitions with larger extinction coefficients, both of which are expected to produce larger Verdet constants under Serber's model of MCB. In addition, the weaker absorption band at 790 nm in **C_{12}-HPHAC$^{+\bullet}$** displays a potential C-term line shape, whereas the analogous band at 630 nm in **C_{12}-HPHAC^{+2}** shows an A-term line shape. Again, this agrees with the Serber model, where only paramagnetic species can exhibit a C-term response.

The solid-state magneto-optical properties are of primary interest, and neutral **C_{12}-HPHAC** was spin-coated to create optical-quality thin films with no observable birefringent domains by polarized-light optical microscopy (POM). As expected from solution measurements, these films did not display a significant Faraday rotation from 400 to 1000 nm. When the spin-coated films of neutral **C_{12}-HPHAC** were left standing overnight or the solution was drop-cast instead of spin-coated, the formation of birefringent crystalline domains was observed by POM (Figure 5a). Differential scanning calorimetry (DSC) (Figure S18a) revealed a melting point from the crystalline phase to an isotropic liquid at 47 °C and no LC phases were detected via DSC or POM. Samples of neutral **C_{12}-HPHAC** that were annealed at 60 °C and cooled down to 20 °C displayed the formation of large fibrils (Figure 5b).

When solutions containing **C_{12}-HPHAC$^{+\bullet}$** were cast into thin film samples, disproportionation to the neutral and dication species was observed. A 1:1 solution of **C_{12}-HPHAC** and $NOBF_4$ in dichloromethane that was spin-coated to form a thin film showed UV−Vis and Faraday rotation spectra with features consistent with the formation of **C_{12}-HPHAC^{+2}**. Consistently, both the absorption intensity and Verdet constants are half the magnitude of that exhibited by thin films prepared from a 1:2 solution of **C_{12}-HPHAC** and $NOBF_4$ (Figure S17). Similar results were obtained when using $SbCl_5$ as an oxidant. Disproportionation was not observed in analogous crystalline peralkylated HPHAC,[15] suggesting that the liquid crystallinity of C_{12}-HPHAC or its enhanced solubility enabling homogeneous solution state oxidation may allow for disproportionation inaccessible in similar systems. As a result of this complexity, **C_{12}-HPHAC$^{+\bullet}$** was not studied further as a solid-state Faraday rotator. The **C_{12}-HPHAC^{+2}** yields a larger Faraday rotation and also has the

https://doi.org/10.1021/jacsau.3c00212
JACS Au 2023, 3, 1965−1974

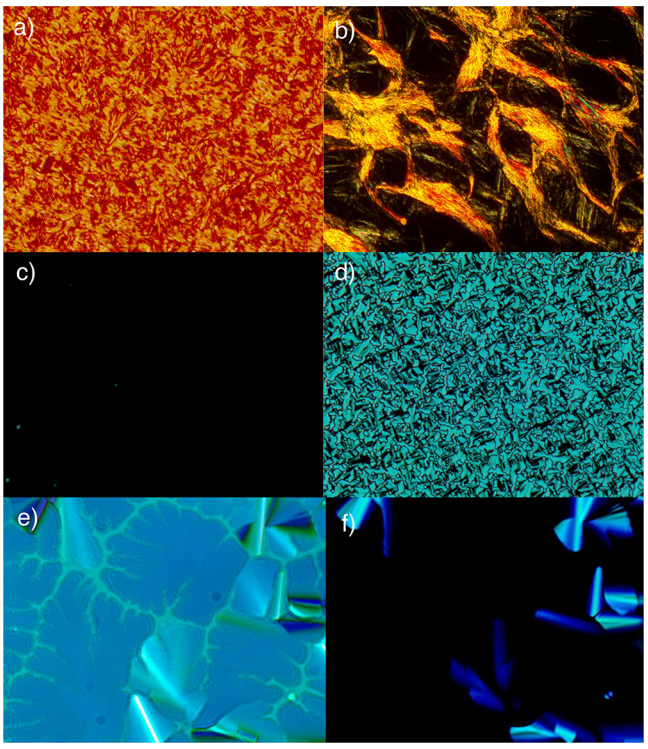

Figure 5. Optical microscopy images at 10× magnification demonstrating the effect of thermal annealing on (a) the drop-casted film of neutral C_{12}-**HPHAC** viewed under crossed polarizing filters, (b) the thermally annealed (60 °C) film of neutral C_{12}-**HPHAC** viewed under crossed polarizing filters, (c) the spin-coated film of mixed C_{12}-**HPHAC**/C_{12}-**HPHAC**$^{+2}$ composition viewed under crossed polarizing filters, (d) the drop-casted film of mixed C_{12}-**HPHAC**/C_{12}-**HPHAC**$^{+2}$ composition viewed under crossed polarizing filters, (e) the thermally annealed (110 °C) film of mixed C_{12}-**HPHAC**/C_{12}-**HPHAC**$^{+2}$ composition viewed without crossed polarizing filters, and (f) the thermally annealed film (110 °C) of mixed C_{12}-**HPHAC**/C_{12}-**HPHAC**$^{+2}$ composition viewed under crossed polarizing filters. All images were taken with samples at room temperature.

advantage of superior air and moisture stability. We find that dichloromethane solutions of C_{12}-**HPHAC**$^{+\bullet}$ significantly decompose after 2 weeks of exposure to ambient conditions, whereas both the solution and thin film of C_{12}-**HPHAC**$^{+2}$ showed no significant degradation and loss in MO rotation over the same period. This result is likely due to the reactivity of the cation radical toward water or oxygen, leading to decomposition products with lower orbital symmetry.

Films containing C_{12}-**HPHAC**$^{+2}$ produced by spin-coating and drop-casting were analyzed by POM. We find that pure C_{12}-**HPHAC**$^{+2}$ prepared via the addition of 3 equiv of $SbCl_5$ does not exhibit birefringence domains under POM. Although birefringence is observed directly after the initial preparation via drop-casting (Figure S19), the texture disappears within 1 h and is not observed via POM again after thermal annealing processes, or with mechanical probing, suggesting an isotropic organization. Interestingly, a DSC thermogram of the sample shows two distinct transitions at 0 and 51 °C, likely associated with ordering (crystallization) of the sidechains and a crystalline transition, respectively. Alternatively, we investigated partial oxidation of C_{12}-**HPHAC** using only 2 equiv of $SbCl_5$, leading to a mixed C_{12}-**HPHAC**/C_{12}-**HPHAC**$^{+2}$ composition in the solid state after disproportionation of the cation radical. It is estimated that the ratio of C_{12}-**HPHAC**$^{+2}$ to C_{12}-**HPHAC** is about 2:1 based on the added equivalents of oxidant and assuming that full disproportionation to these two species occurs. In the case of the mixed valent C_{12}-**HPHAC**/C_{12}-**HPHAC**$^{+2}$ film, persistent liquid crystalline properties were observed. We find that the disorder originating from a mixed composition of neutral and dication species leads to the formation of a well-behaved LC phase, which is not observed in pure C_{12}-**HPHAC**$^{+2}$. Both samples prepared using 2 and 3 equiv of $SbCl_5$ were investigated for their Faraday rotation; however, the following discussion focuses on the mixed composition and its morphology. Spin-coated thin films of mixed C_{12}-**HPHAC**/C_{12}-**HPHAC**$^{+2}$ displayed no birefringent domains under cross polarizers, suggesting a quenched amorphous glass morphology (Figure 5c). However, when these films were left to stand overnight, small birefringent domains consistent with a LC organization appear. Similar

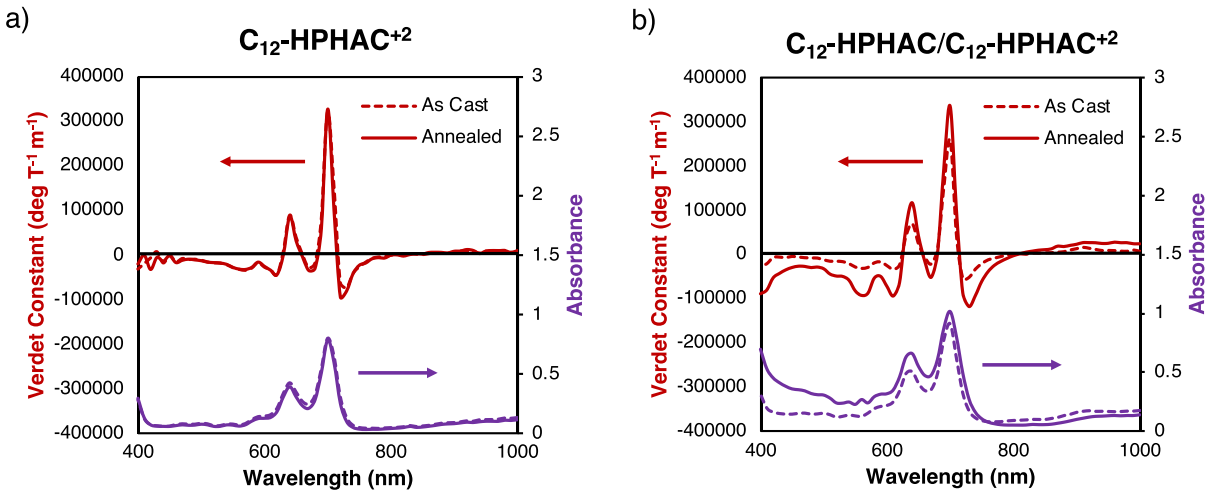

Figure 6. UV−Vis spectra (purple) and associated Faraday rotation responses (red) of thin films prepared from dichloromethane solutions of (a) a 1:2 mixture and (b) a 1:3 mixture of C_{12}-**HPHAC** and $SbCl_5$ when spin-coated (dotted lines), annealed at 110 °C, and subsequently slowly cooled down to 20 °C at a rate of 1°/min (solid lines). The films were prepared from a 10 mg/mL solution of C_{12}-**HPHAC** in dichloromethane to which the appropriate equivalents of $SbCl_5$ were added. The film thickness is 220 nm.

https://doi.org/10.1021/jacsau.3c00212
JACS Au 2023, 3, 1965−1974

optical features are observed directly when the solution of **C_{12}-HPHAC** with 2 equiv of $SbCl_5$ was drop-cast (Figure 5d), suggesting that LC organization is preferred over a kinetic disordered morphology produced by spin-coating. DSC thermograms revealed no discernable transitions other than the one at −27 °C that is associated with ordering (crystallization) of the sidechains. When the sample was heated under POM observation, a clear isotropic transition was observed at 95 °C, with the loss of the birefringent domains. Samples were heated at 110 °C and subsequently slowly cooled down to 20 °C at a rate of 1°/min, and under these conditions, the LC domains are largely homeotropically aligned with the columnar (optic) axis aligned normal to the surface. This feature and a small number of rectilinear birefringent domains are suggestive of a columnar LC phase (Figure 5e,f). The absence of an observable peak at that temperature in the DSC thermogram (Figure S18b) indicates a low clearing enthalpy and perhaps a broader transition as a result of the fact that the phase contains a dication and neutral **C_{12}-HPHAC** mixture and $SbCl_3$ species in addition to disordered $SbCl_6$ counterions. Considering the large diameter of the **C_{12}-HPHAC** disc, it is also possible that a discotic nematic phase is present at elevated temperatures, which would explain the difficulty in measuring a transition peak in the DSC and may account for the fact that the columnar phase spontaneously forms large homeotropic domains without any surface treatments or methods to induce alignment. Grazing incidence small-angle X-ray scattering (GISAXS) measurements were conducted to confirm the nature of the columnar phase and if a discotic nematic phase is present (Figure S23). A peak at d = 3.9 is observed under all conditions investigated and is associated with the spacing of the aromatic cores. We did not detect any anisotropy in this diffuse diffraction, which would confirm alignment as the result of a discotic nematic phase. The complex mixed valence nature of the LC results in slow organization of the structures into columnar phases. However, we observe sharp low angle peaks at 18.9 and 16.2 Å consistent with the (200) and (110) diffractions of a Col_r phase (a = 18.0 Å, b = 37.8 Å).

We were interested in investigating the impact of order imposed by the liquid crystalline state on the Faraday rotation of **C_{12}-HPHAC^{+2}**. Figure 6a presents the absorption and Faraday rotation spectra of a 220 nm spin-coated film of pure **C_{12}-HPHAC^{+2}** prepared using 3 equiv of $SbCl_5$. This sample displayed a maximum Verdet constant of 3.25 × 10^5 deg T^{-1} m^{-1} at 700 nm (dotted lines). Upon thermal treatment at 110 °C followed by slowly cooling down to 20 °C at a rate of 1°/min, no significant difference in both the absorption and Faraday rotation spectra was observed (solid lines) owing to the absence of an LC phase that could lead to favorable molecular alignment. Next, a spin-coated thin film of **C_{12}-HPHAC/C_{12}-HPHAC^{+2}** prepared using 2 equiv of $SbCl_5$ that displayed a POM image devoid of birefringence (i.e., similar to Figure 5c) was measured and yielded the Faraday rotation spectra presented in Figure 6b (dotted lines). This sample displayed maximum Verdet constants of 2.58 × 10^5 deg T^{-1} m^{-1} at 700 nm in the positive region and −0.55 × 10^5 deg T^{-1} m^{-1} at 720 nm in the negative region. As expected, the maximum Verdet constant at 700 nm for the **C_{12}-HPHAC/C_{12}-HPHAC^{+2}** film is smaller than the pure **C_{12}-HPHAC^{+2}** film as the content of **C_{12}-HPHAC^{+2}** is lesser. When the sample was annealed at 110 °C and then allowed to cool down slowly to 20 °C at a rate of 1°/min, the POM image displayed a similar texture to the one shown in Figure 5f and a significant increase in Faraday rotation was observed (solid lines). The Verdet constant at 700 nm increased to 3.36 × 10^5 deg T^{-1} m^{-1}, a gain of 30%, whereas the Verdet constant at 720 nm increased to −1.17 × 10^5 deg. T^{-1} m^{-1}, a gain of 105%. Note that even with roughly 2/3 the content in **C_{12}-HPHAC^{+2}**, the mixed **C_{12}-HPHAC/C_{12}-HPHAC^{+2}** film outperformed the pure **C_{12}-HPHAC^{+2}** film in its magneto-optical properties. The 700 nm value is one of the highest for an organic Faraday rotator in the UV−Vis range to date. We attribute the gains in Verdet constant to a homeotropic alignment of the chromophoric magneto-optically active cores relative to the glass surfaces, which places the net polarization perpendicular to the applied external magnetic field. To understand the impact of molecular alignment on Faraday rotation, an examination of the semi-quantitative expression of the magnitude of the A-term in Serber's model of MCB is needed.[23] In the expression, the first factor $\langle j|m_z|j\rangle - \langle n|m_z|n\rangle$ indicates that the Faraday A-term is related to the difference between the ground- and excited-state magnetic moments for each component transition. Note that only changes in magnetic dipole moments along the z-axis will impact the A-term magnitude. The second factor in the expression $Im\{\langle n|\mu_x|j\rangle\langle j|\mu_y|n\rangle\}$ describes the imaginary part of the transition dipole moments in the xy-plane. The real component of the transition dipole moments relates to the absorptivity of the transition; and so, in many systems such as porphyrinoids and **C_{12}-HPHAC^{+2}**, the magnitude of the Faraday A-term is proportional to the molar absorptivity. Both factors refer to the coordinate system, indicating that the orientation of the magnetic dipole moments and the electric transition dipole moments matter, and so, molecular order along specific sample axes may yield enhanced Faraday rotation. Note that these conclusions also hold for the Faraday C-term. Therefore, we postulate that the molecular orientation reached when the chromophoric discotic cores are aligned perpendicular to the magnetic field direction leads to favorable orientations of both the magnetic dipole and electric transition dipole moments to give optimally large Verdet constants. Note that the annealed **C_{12}-HPHAC/C_{12}-HPHAC^{+2}** sample also exhibits UV−Vis absorption of greater magnitude, which is to be expected as well. However, the increase in maximum absorption does not linearly correlate with the gain in Verdet constants. Indeed, the maximum absorbance in the annealed film increases by 11% at 700 nm, from 0.91 to 1.01, and by 40%, from 0.32 to 0.45, at 720 nm, whereas the Verdet constants display a three-fold larger increase. This suggests that the gain is not merely the result of a thicker film after the annealing process or a linear correlation between optical and magneto-optical properties.

CONCLUSIONS

In summary, this study has demonstrated the viability of **HPHAC** as Faraday rotators and the use of LC phases to increase the Faraday rotation of MO active organic materials. The largest Verdet constants observed in both **C_{12}-HPHAC$^{+\bullet}$** and **C_{12}-HPHAC^{+2}** are attributed to the Faraday A-term. Thin films containing **C_{12}-HPHAC^{+2}** exhibit some of the largest Verdet constants reported in organic materials, as high as 3.36 × 10^5 deg T^{-1} m^{-1}. Neutral **C_{12}-HPHAC** does not exhibit an LC phase, but a **C_{12}-HPHAC/C_{12}-HPHAC^{+2}** composition obtained from oxidation with 2 equiv of $SbCl_5$ displays a discotic columnar LC phase that has rectangular symmetry and possibly a discotic nematic LC phase, which can assist in

https://doi.org/10.1021/jacsau.3c00212
JACS Au 2023, 3, 1965−1974

creating homeotropically aligned thin films, resulting in significant gains in Verdet constants of up to 105%. The results obtained in this study provide a strong foundation for further research on the development and optimization of liquid crystalline organic Faraday rotators, with the aim of achieving improved performance and practical applications. For resonance-enhanced organic Faraday rotators to be utilized in practical applications, the optimization of parameters such as molecular alignment as well as the obtention of larger Verdet constants and thicker films will be needed.

METHODS

The syntheses are detailed in the Supporting Information. For solid-state samples, thin films were prepared from a mixture of neutral **C_{12}-HPHAC** only or with the addition of an oxidizing agent via spin-coating or drop-casting onto a high-precision #1.5H glass coverslip (170 ± 5 μm). Typically, solutes were dissolved in dichloromethane, with the **C_{12}-HPHAC** concentration set between 5 and 20 mg mL^{-1} and with the appropriate amount of oxidizing agent added, before spin-coating at 1000 rpm or drop-casting. Only samples of high optical quality were measured, and the quality was validated by POM images (Leica DMRXP) taken of the thin films in transmission. The thickness of each thin film was determined using contact profilometry (Dektak 6M Profilometer) and ranged from 100 to 400 nm. Thermal annealing was conducted by placing a second high-precision #1.5H glass coverslip on top of the film and heating the sample on a Linkam TMS 94 hot stage with the following temperature profile: heated from 20 °C to above the respective isotropic transitions at 30 °C min^{-1} and then cooled to 20 °C at 1 °C min^{-1} under an ambient atmosphere. For liquid samples, solutions were loaded into a PTFE-stoppered quartz cuvette with a 1.0 mm light path. MCB and UV−vis spectra were obtained from a home-built measurement system based on established designs[43] and a Cary 60 UV−Vis spectrophotometer. Faraday rotation results are reported as the full spectra, spanning from 400 to 1000 nm with incremental measurements at every 10 nm for both solution- and solid-state samples. The measured property for solid-state spectra is the Verdet constant (deg T^{-1} m^{-1}), and solution-state measurements are reported as the mass-specific magnetic rotation (deg L g^{-1} T^{-1} m^{-1}). The Faraday system and experimental details regarding MCB measurements are described in a previous report.[43]

ASSOCIATED CONTENT

Supporting Information

The Supporting Information is available free of charge at https://pubs.acs.org/doi/10.1021/jacsau.3c00212.

Details of the experimental procedures, additional Faraday rotation and absorption spectra, DSC thermograms, POM images, and DFT and NICS calculations (PDF)

AUTHOR INFORMATION

Corresponding Author

Timothy M. Swager − *Department of Chemistry, Massachusetts Institute of Technology, Cambridge, Massachusetts 02139, United States; Institute for Soldier Nanotechnologies, Cambridge, Massachusetts 02139, United States;* orcid.org/0000-0002-3577-0510; Email: tswager@mit.edu

Author

Léo Delage-Laurin − *Department of Chemistry, Massachusetts Institute of Technology, Cambridge, Massachusetts 02139, United States; Institute for Soldier Nanotechnologies, Cambridge, Massachusetts 02139, United States;* orcid.org/0000-0002-9174-5416

Complete contact information is available at: https://pubs.acs.org/10.1021/jacsau.3c00212

Notes

The authors declare no competing financial interest.

ACKNOWLEDGMENTS

This research was funded by the Air Force Office of Scientific Research grant: 17RT0904; FA9550-18-1-0341. We would like to thank Prof. Richard Y. Liu for providing the DFT and NICS calculations.

REFERENCES

(1) Wang, X.-Y.; Yao, X.; Narita, A.; Müllen, K. Heteroatom-Doped Nanographenes with Structural Precision. *Acc. Chem. Res.* **2019**, *52*, 2491−2505.

(2) Stępień, M.; Gońka, E.; Żyła, M.; Sprutta, N. Heterocyclic Nanographenes and Other Polycyclic Heteroaromatic Compounds: Synthetic Routes, Properties, and Applications. *Chem. Rev.* **2017**, *117*, 3479−3716.

(3) Jiang, M.-J.; Xiao, W.-J.; Huang, J.-C.; Li, W.-S.; Mo, Y.-Q. Diindole[3,2-b:4,5-B′]Pyrrole as a Chromophore Containing Three Successively Fused Pyrroles: Synthesis Optoelectronic Properties and π-Functionalization. *Tetrahedron* **2016**, *72*, 979−984.

(4) Wang, L.; Lin, L.; Yang, J.; Wu, Y.; Wang, H.; Zhu, J.; Yao, J.; Fu, H. Singlet Fission in a Pyrrole-Fused Cross-Conjugated Skeleton with Adaptive Aromaticity. *J. Am. Chem. Soc.* **2020**, *142*, 10235−10239.

(5) Li, Y.; Xu, L.; Jiang, R.; Liu, H.; Li, Y. Synthesis of Amino-Substituted Pyrrole-Fused Perylenebis(Dicarboximide) Derivatives by a One-Pot Azidation/Reduction/Cyclization. *Eur. J. Org. Chem.* **2013**, *2013*, 7076−7082.

(6) Wang, W.; Hanindita, F.; Tanaka, Y.; Ochiai, K.; Sato, H.; Li, Y.; Yasuda, T.; Ito, S. π-Extended Pyrrole-Fused Heteropine: Synthesis, Properties, and Application in Organic Field-Effect Transistors. *Angew. Chem., Int. Ed.* **2023**, *62*, No. e202218176.

(7) Sasaki, Y.; Takase, M.; Kobayashi, N.; Mori, S.; Ohara, K.; Okujima, T.; Uno, H. Radially π-Extended Pyrrole-Fused Azacoronene: A Series of Crystal Structures of HPHAC with Various Oxidation States. *J. Org. Chem.* **2021**, *86*, 4290−4295.

(8) Wu, D.; Descalzo, A. B.; Weik, F.; Emmerling, F.; Shen, Z.; You, X.-Z.; Rurack, K. A Core-Modified Rubyrin with Meso-Aryl Substituents and Phenanthrene-Fused Pyrrole Rings: A Highly Conjugated Near-Infrared Dye and Hg2+ Probe. *Angew. Chem., Int. Ed.* **2008**, *47*, 193−197.

(9) Mukherjee, S.; Hazra, S.; Chowdhury, S.; Sarkar, S.; Chattopadhyay, K.; Pramanik, A. A Novel Pyrrole Fused Coumarin Based Highly Sensitive and Selective Fluorescence Chemosensor for Detection of Cu2+ Ions and Applications towards Live Cell Imaging. *J. Photochem. Photobiol., A* **2018**, *364*, 635−644.

(10) De los Santos, M. G.; Cua-Basulto, M.; Huepalcalco, A.; Delit, W.; Sandoval-Ramírez, J.; López-Torres, A.; Ruiz-Sánchez, E.; Fernández-Herrera, M. A. Fused Pyrroles in Cholestane and Norcholestane Side Chains: Acaricidal and Plant Growth-Promoting Effects. *Molecules* **2022**, *27*, 8466.

(11) Abd El-Hameed, R. H.; Sayed, A. I.; Mahmoud Ali, S.; Mosa, M. A.; Khoder, Z. M.; Fatahala, S. S. Synthesis of Novel Pyrroles and Fused Pyrroles as Antifungal and Antibacterial Agents. *J. Enzyme Inhib. Med. Chem.* **2021**, *36*, 2183−2198.

(12) Said Fatahala, S.; Hasabelnaby, S.; Goudah, A.; Mahmoud, G.; Hameed, H. A.-E.; R. Pyrrole and Fused Pyrrole Compounds with Bioactivity against Inflammatory Mediators. *Molecules* **2017**, *22*, 461.

(13) Takase, M.; Enkelmann, V.; Sebastiani, D.; Baumgarten, M.; Müllen, K. Annularly Fused Hexapyrrolohexaazacoronenes: An Extended π System with Multiple Interior Nitrogen Atoms Displays Stable Oxidation States. *Angew. Chem., Int. Ed.* **2007**, *46*, 5524−5527.

(14) Oki, K.; Takase, M.; Mori, S.; Shiotari, A.; Sugimoto, Y.; Ohara, K.; Okujima, T.; Uno, H. Synthesis, Structures, and Properties of Core-Expanded Azacoronene Analogue: A Twisted π-System with Two N-Doped Heptagons. *J. Am. Chem. Soc.* **2018**, *140*, 10430−10434.
(15) Oki, K.; Takase, M.; Kobayashi, N.; Uno, H. Synthesis and Characterization of Peralkylated Pyrrole-Fused Azacoronene. *J. Org. Chem.* **2021**, *86*, 5102−5109.
(16) Lazerges, M.; Jouini, M.; Hapiot, P.; Guiriec, P.; Lacaze, P.-C. Mechanism of Pyrrolyl Oxidation in Star-Shaped Compounds. *J. Phys. Chem. A* **2003**, *107*, 5042−5048.
(17) Navakouski, M.; Zhylitskaya, H.; Chmielewski, P. J.; Lis, T.; Cybińska, J.; Stępień, M. Stereocontrolled Synthesis of Chiral Heteroaromatic Propellers with Small Optical Bandgaps. *Angew. Chem., Int. Ed.* **2019**, *58*, 4929−4933.
(18) Żyła, M.; Gońka, E.; Chmielewski, J.; Cybińska, J.; Stępień, M. Synthesis of a Peripherally Conjugated 5-6-7 Nanographene. *Chem. Sci.* **2016**, *7*, 286−294.
(19) Oki, K.; Takase, M.; Mori, S.; Uno, H. Synthesis and Isolation of Antiaromatic Expanded Azacoronene via Intramolecular Vilsmeier-Type Reaction. *J. Am. Chem. Soc.* **2019**, *141*, 16255−16259.
(20) Żyła-Karwowska, M.; Zhylitskaya, H.; Cybińska, J.; Lis, T.; Chmielewski, P. J.; Stępień, M. An Electron-Deficient Azacoronene Obtained by Radial π Extension. *Angew. Chem., Int. Ed.* **2016**, *55*, 14658−14662.
(21) Takase, M.; Ueno, A.; Oki, K.; Matsumoto, H.; Mori, S.; Okujima, T.; Uno, H. Tropo(Thio)Ne-Embedded HomoHPHACs: Does the Tropylium Cation Induce Global Antiaromaticity in Expanded Hexapyrrolohexaazacoronene? *Chem. Commun.* **2022**, *58*, 3366−3369.
(22) Sasaki, Y.; Takase, M.; Okujima, T.; Mori, S.; Uno, H. Synthesis and Redox Properties of Pyrrole- and Azulene-Fused Azacoronene. *Org. Lett.* **2019**, *21*, 1900−1903.
(23) Nelson, Z.; Delage-Laurin, L.; Swager, T. M. ABCs of Faraday Rotation in Organic Materials. *J. Am. Chem. Soc.* **2022**, *144*, 11912−11926.
(24) Longair, M. S. *High Energy Astrophysics*, 3rd ed.; Cambridge University Press: Cambridge; New York, 2012.
(25) Oppermann, N.; Junklewitz, H.; Greiner, M.; Enßlin, T. A.; Akahori, T.; Carretti, E.; Gaensler, B. M.; Goobar, A.; Harvey-Smith, L.; Johnston-Hollitt, M.; Pratley, L.; Schnitzeler, D. H. F. M.; Stil, J. M.; Vacca, V. Estimating Extragalactic Faraday Rotation. *Astron. Astrophys.* **2015**, *575*, A118.
(26) Ferrière, K.; West, J. L.; Jaffe, T. R. The Correct Sense of Faraday Rotation. *Mon. Not. R. Astron. Soc.* **2021**, *507*, 4968−4982.
(27) Chang, Y. Y.; Cheng, X.; Hannasch, A.; LaBerge, M.; Shaw, J. M.; Weichman, K.; Welch, J.; Bernstein, A.; Henderson, W.; Zgadzaj, R.; Downer, M. C. Faraday Rotation Study of Plasma Bubbles in GeV Wakefield Accelerators. *Phys. Plasmas* **2021**, *28*, 123105.
(28) Park, K.; Blackman, E. G. Effect of Plasma Composition on the Interpretation of Faraday Rotation. *Mon. Not. R. Astron. Soc.* **2010**, *403*, 1993−1998.
(29) Pisarczyk, T.; Rupasov, A. A.; Sarkisov, G. S.; Shikanov, A. S. Faraday-Rotation Method for Magnetic-Field Diagnostics in a Laser Plasma. *J. Sov. Laser Res.* **1990**, *11*, 1−32.
(30) Cao, Y.; Liu, K.; Wang, R.; Gao, X.; Kang, R.; Fang, Y.; Chen, W. NO2 Sensor Based on Faraday Rotation Spectroscopy Using Ring Array Permanent Magnets. *Anal. Chem.* **2023**, *95*, 1680−1685.
(31) Cheng, L.; Han, J.; Guo, Z.; Jin, L.; Guan, B.-O. Faraday-Rotation-Based Miniature Magnetic Field Sensor Using Polarimetric Heterodyning Fiber Grating Laser. *Opt. Lett.* **2013**, *38*, 688−690.
(32) Sun, L.; Jiang, S.; Marciante, J. R. All-Fiber Optical Magnetic-Field Sensor Based on Faraday Rotation in Highly Terbium-Doped Fiber. *Opt. Express* **2010**, *18*, 5407−5412.
(33) Simpson, D. A.; Tetienne, J.-P.; McCoey, J. M.; Ganesan, K.; Hall, L. T.; Petrou, S.; Scholten, R. E.; Hollenberg, L. C. L. Magneto-Optical Imaging of Thin Magnetic Films Using Spins in Diamond. *Sci. Rep.* **2016**, *6*, 22797.
(34) Deng, Y.; Cheng, Y.; Xuan, L.; Zeng, Z. Principles of Magneto-Optic Imaging and Its Applications. In *Integrated Imaging and Vision Techniques for Industrial Inspection: Advances and Applications*; Liu, Z., Ukida, H., Ramuhalli, P., Niel, K., Eds.; Advances in Computer Vision and Pattern Recognition; Springer: London, 2015; pp. 483−536.
(35) Deng, Y.; Liu, X. Magneto-Optic Imaging for Aircraft Skins Inspection: A Probability of Detection Study of Simulated and Experimental Image Data. In *2011 IEEE Conference on Prognostics and Health Management*; 2011; pp. 1−8.
(36) Bomke, H. A.; Harmatz, M. Enhanced Faraday Effect and Its Application to Optical Communication. *Appl. Opt.* **1977**, *16*, 751−755.
(37) Kobayashi, N.; Ikeda, K.; Gu, B.; Takahashi, S.; Masumoto, H.; Maekawa, S. Giant Faraday Rotation in Metal-Fluoride Nanogranular Films. *Sci. Rep.* **2018**, *8*, 4978.
(38) Dötsch, H.; Bahlmann, N.; Zhuromskyy, O.; Hammer, M.; Wilkens, L.; Gerhardt, R.; Hertel, P.; Popkov, A. F. Applications of Magneto-Optical Waveguides in Integrated Optics: Review. *JOSA B* **2005**, *22*, 240−253.
(39) Palashov, O. V.; Zheleznov, D. S.; Voitovich, A. V.; Zelenogorsky, V. V.; Kamenetsky, E. E.; Khazanov, E. A.; Martin, R. M.; Dooley, K. L.; Williams, L.; Lucianetti, A.; Quetschke, V.; Mueller, G.; Reitze, D. H.; Tanner, D. B.; Genin, E.; Canuel, B.; Marque, J. High-Vacuum-Compatible High-Power Faraday Isolators for Gravitational-Wave Interferometers. *JOSA B* **2012**, *29*, 1784−1792.
(40) Shoji, Y.; Mizumoto, T. Silicon Waveguide Optical Isolator with Directly Bonded Magneto-Optical Garnet. *Appl. Sci.* **2019**, *9*, 609.
(41) Yasuhara, R.; Snetkov, I.; Starobor, A.; Zheleznov, D.; Palashov, O.; Khazanov, E.; Nozawa, H.; Yanagitani, T. Terbium Gallium Garnet Ceramic Faraday Rotator for High-Power Laser Application. *Opt. Lett.* **2014**, *39*, 1145−1148.
(42) Molina, P.; Vasyliev, V.; Víllora, E. G.; Shimamura, K. CeF_3 and PrF_3 as UV-Visible Faraday Rotators. *Opt. Express* **2011**, *19*, 11786.
(43) Nelson, Z.; Delage-Laurin, L.; Peeks, M. D.; Swager, T. M. Large Faraday Rotation in Optical-Quality Phthalocyanine and Porphyrin Thin Films. *J. Am. Chem. Soc.* **2021**, *143*, 7096−7103.
(44) Vandendriessche, S.; Van Cleuvenbergen, S.; Willot, P.; Hennrich, G.; Srebro, M.; Valev, V. K.; Koeckelberghs, G.; Clays, K.; Autschbach, J.; Verbiest, T. Giant Faraday Rotation in Mesogenic Organic Molecules. *Chem. Mater.* **2013**, *25*, 1139−1143.
(45) Vleugels, R.; Steverlynck, J.; Brullot, W.; Koeckelberghs, G.; Verbiest, T. Faraday Rotation in Discotic Liquid Crystals by Long-Range Electron Movement. *J. Phys. Chem. C* **2019**, *123*, 9382−9387.
(46) Delage-Laurin, L.; Nelson, Z.; Swager, T. M. C-Term Faraday Rotation in Metallocene Containing Thin Films. *ACS Appl. Mater. Interfaces* **2021**, *13*, 25137−25142.
(47) Takase, M.; Narita, T.; Fujita, W.; Asano, M. S.; Nishinaga, T.; Benten, H.; Yoza, K.; Müllen, K. Pyrrole-Fused Azacoronene Family: The Influence of Replacement with Dialkoxybenzenes on the Optical and Electronic Properties in Neutral and Oxidized States. *J. Am. Chem. Soc.* **2013**, *135*, 8031−8040.
(48) Schenz, A. F.; Neff, V. D.; Schenz, T. W. Faraday Rotation in Nematic Liquids. *Mol. Cryst. Liq. Cryst.* **1973**, *23*, 59−67.
(49) Guernion, L.; Hayes, W. 3- and 3,4-Substituted Pyrroles and Thiophenes and Their Corresponding Polymers - A Review. *Curr. Org. Chem.* **2004**, *8*, 637−651.
(50) Bray, B. L.; Mathies, P. H.; Naef, R.; Solas, D. R.; Tidwell, T. T.; Artis, D. R.; Muchowski, J. M. N-(Triisopropylsilyl)Pyrrole. A Progenitor "Par Excellence" of 3-Substituted Pyrroles. *J. Org. Chem.* **1990**, *55*, 6317−6328.
(51) Melling, D.; Wilson, S. A.; Jager, E. W. H. Controlling the Electro-Mechanical Performance of Polypyrrole through 3- and 3,4-Methyl Substituted Copolymers. *RSC Adv.* **2015**, *5*, 84153−84163.
(52) Ichimura, K.; Ichikawa, S.; Imamura, K. Syntheses of 3,4-Dimethylpyrrole. *Bull. Chem. Soc. Jpn.* **1976**, *49*, 1157−1158.

https://doi.org/10.1021/jacsau.3c00212
JACS Au 2023, 3, 1965−1974

(53) Alsharif, M. A.; Raja, Q. A.; Majeed, N. A.; Jassas, R. S.; Alsimaree, A. A.; Sadiq, A.; Naeem, N.; Mughal, E. U.; Alsantali, R. I.; Moussa, Z.; Ahmed, S. A. DDQ as a Versatile and Easily Recyclable Oxidant: A Systematic Review. *RSC Adv.* **2021**, *11*, 29826−29858.
(54) Zhai, L.; Shukla, R.; Rathore, R. Oxidative C−C Bond Formation (Scholl Reaction) with DDQ as an Efficient and Easily Recyclable Oxidant. *Org. Lett.* **2009**, *11*, 3474−3477.
(55) LeGoff, E.; Chamberlin, S. K.; LeGoff, E. General Synthesis of Octaalkylporphyrins. *Heterocycles* **1979**, *12*, 1567.
(56) Shearman, G. C.; Yahioglu, G.; Kirstein, J.; Milgrom, L. R.; Seddon, J. M. Synthesis and Phase Behaviour of *β*-Octaalkyl Porphyrins. *J. Mater. Chem.* **2009**, *19*, 598−604.
(57) Shevchuk, S. V.; Davis, J. M.; Sessler, J. L. Synthesis of Sapphyrins via a '3+1+1' Procedure. *Tetrahedron Lett.* **2001**, *42*, 2447−2450.
(58) Milgram, B. C.; Eskildsen, K.; Richter, S. M.; Scheidt, W. R.; Scheidt, K. A. Microwave-Assisted Piloty−Robinson Synthesis of 3,4-Disubstituted Pyrroles. *J. Org. Chem.* **2007**, *72*, 3941−3944.
(59) Beh, M. H. R.; Figliola, C.; Lund, K.-L. A. R.; Kajetanowicz, A. K.; Johnsen, A. E.; Aronitz, E. M.; Thompson, A. Regioselective Substituent Effects upon the Synthesis of Dipyrrins from 2-Formyl Pyrroles. *Can. J. Chem.* **2018**, *96*, 779−784.
(60) Brandsma, L.; Meijer, J.; Verkruijsse, H. D.; Bokkers, G.; Duisenberg, A. J. M.; Kroon, J. Synthesis, Crystal, and Molecular Structure of 3,4-Di-t-Butylthiophen. *J. Chem. Soc., Chem. Commun.* **1980**, 922.
(61) Rathore, R.; Kumar, A. S.; Lindeman, S. V.; Kochi, J. K. Preparation and Structures of Crystalline Aromatic Cation-Radical Salts. Triethyloxonium Hexachloroantimonate as a Novel (One-Electron) Oxidant. *J. Org. Chem.* **1998**, *63*, 5847−5856.

https://doi.org/10.1021/jacsau.3c00212
JACS Au 2023, 3, 1965−1974